Atherosclerosis Inflammation Imaging with ^{18}F-FDG PET: Carotid, Iliac, and Femoral Uptake Reproducibility, Quantification Methods, and Recommendations

James H.F. Rudd*[1], Kelly S. Myers*[1], Sameer Bansilal[2], Josef Machac[3], Cathy Anne Pinto[4], Christopher Tong[4], Ash Rafique[3], Richard Hargeaves[4], Michael Farkouh[2], Valentin Fuster[5], and Zahi A. Fayad[1]

[1]Imaging Science Laboratories, Mount Sinai School of Medicine, New York, New York; [2]Cardiovascular Imaging Clinical Trials Unit, Mount Sinai School of Medicine, New York, New York; [3]Division of Nuclear Medicine, Department of Radiology, Mount Sinai School of Medicine, New York, New York; [4]Mount Sinai School of Medicine, New York, New York, and Merck Research Laboratories, Rahway, New Jersey; and [5]The Zena and Michael A. Wiener Cardiovascular Institute and Marie-Josée and Henry R. Kravis Cardiovascular Health Center, Mount Sinai School of Medicine, New York, New York

Atherosclerosis imaging with ^{18}F-FDG PET is useful for tracking inflammation within plaque and monitoring the response to drug therapy. Short-term reproducibility of this technique in peripheral artery disease has not been assessed, and the optimal method of ^{18}F-FDG quantification is still debated. We imaged 20 patients with vascular disease using ^{18}F-FDG PET twice, 14 d apart, and used these data to assess reproducibility measures and compare 2 methods of ^{18}F-FDG uptake measurement. We also reviewed the literature on quantification methods to determine the optimal measures of arterial ^{18}F-FDG uptake for future studies. **Methods:** Twenty patients with vascular disease underwent PET/CT of the iliac, femoral, and carotid arteries 90 min after ^{18}F-FDG administration. In 19 patients, repeat testing was performed at 2 wk. Coregistration and attenuation correction were performed with CT. Vessel ^{18}F-FDG uptake was measured as both the mean and maximum blood-normalized standardized uptake value (SUV), known as the target-to-background ratio (TBR). We assessed interscan, interobserver, and intraobserver agreement. **Results:** Nineteen patients completed both imaging sessions. The carotid and peripheral arteries all have excellent short-term reproducibility of the ^{18}F-FDG signal, with intraclass correlation coefficients all greater than 0.8 for all measures of reproducibility. Both mean and maximum TBR measurements for quantifying ^{18}F-FDG uptake are equally reproducible. ^{18}F-FDG uptake was significantly higher in the carotid arteries than in both iliac and femoral vessels ($P < 0.001$ for both). **Conclusion:** We found that both mean and maximum TBR in the carotid, iliac, and femoral arteries were highly reproducible. We suggest the mean TBR be used for tracking systemic arterial therapies, whereas the maximum TBR is optimal for detecting and monitoring local, plaque-based therapy.

Key Words: atherosclerosis; positron emission tomography; ^{18}F-FDG; inflammation; methodology

J Nucl Med 2008; 49:871–878
DOI: 10.2967/jnumed.107.050294

Worldwide mortality and morbidity from vascular disease is increasing. The need for novel drugs to halt disease progression and induce regression is urgent. Patients with atherosclerotic peripheral vascular disease have a high incidence of both stroke and acute coronary syndrome (*1*).

Epidemiologic and basic science studies have shown that an individual patient's risk of future clinical events can be approximated from risk-factor scores such as Framingham (*2*). However, the detection of subclinical atherosclerosis by imaging can help to refine risk estimates (*3,4*). Serial monitoring of therapy response during proof-of-concept studies can give an early readout of treatment efficacy, potentially saving the time and cost of continued drug development for therapies that fail during large-scale confirmatory and outcome studies.

The biggest driver for plaque destabilization and clinical adverse events is inflammation (*5*), which occurs devastatingly within the protective fibrous cap of the plaque, where it promotes rupture by enzymatic degradation of the structural integrity of the cap. Although current imaging technologies are able to quantify the extent of disease in terms of luminal obstruction and visualization of some plaque elements, ^{18}F-FDG PET offers a unique noninvasive measure of plaque inflammation. This is because ^{18}F-FDG is retained within plaque macrophages more avidly than within other plaque elements (*6*).

Received Dec. 24, 2007; revision accepted Feb. 28, 2008.
For correspondence or reprints contact either of the following:
James Rudd, ACCI, Box 110, Addenbrokes Hospital, Cambridge CB2 2QQ, U.K.
E-mail: jhfr2@cam.ac.uk
Zahi A. Fayad, ISL, Mount Sinai School of Medicine, One Gustave L. Levy Place, Box 1030, New York, NY 10029.
E-mail: zahi.fayad@mssm.edu
*Contributed equally to this work.

Before being used to track changes in plaque inflammation over time and after therapy, however, the reproducibility of the technique has to be tested. We reported good reproducibility recently in a small group of patients that underwent carotid artery and aortic imaging, with high inter- and intraobserver agreement and low variability of ^{18}F-FDG uptake over 2 wk (*7*).

In the current study, we prospectively imaged for, what is to our knowledge, the first time the iliac and femoral arteries with ^{18}F-FDG PET and determined near-term reproducibility in those arterial beds. Novel interventions for peripheral artery disease are becoming available, and the need to highlight inflamed symptomatic lesions is important (*8,9*). We also present a larger cohort of patients than has been previously studied, who underwent carotid imaging twice over 2 wk, and determine reproducibility statistics for this group. In addition, we compare the reproducibility of 2 different methods of measurement of plaque ^{18}F-FDG uptake and suggest optimal quantification protocols for future drug trials using ^{18}F-FDG PET of atherosclerosis.

MATERIALS AND METHODS

Study Population

To generate widely applicable reproducibility statistics and SD values, we prospectively recruited a heterogeneous group of 20 patients with established or suspected vascular disease (defined as a previous myocardial infarction, stroke, or transient ischemic attack [TIA]; a history of a coronary revascularization procedure; or multiple risk factors for coronary artery disease) from within the Mount Sinai Medical Center. A sample size of 20 patients was calculated using an expected intraclass correlation coefficient (ICC) of 0.7 or greater, with the half-width of the confidence interval equal to 0.3. All patients gave written informed consent, and the study was approved by the Institutional Review Board of the Mount Sinai School of Medicine.

PET/CT

A total of 20 patients was recruited, and 19 completed carotid and leg PET/CT on 2 occasions, 2 wk apart (scan 1 and scan 2). Patient 20 withdrew from the study after the first PET scan because of intercurrent illness. Only the results for the 19 patients who completed both scans are presented. For the final 12 of the 20 patients, the protocol was amended to add femoral artery PET to the existing iliac and carotid protocol.

Imaging was performed using a 16-slice PET/CT scanner (Lightspeed; GE Healthcare), with a 15.5-cm field of view, after patients had fasted for at least 8 h. Blood glucose was checked by finger-stick measurement before ^{18}F-FDG injection. Patients with a prescan glucose level of 200 mg/dL or more were excluded from the study. ^{18}F-FDG (500–600 MBq) was injected intravenously, and patients rested in a quiet room for 90 min. Leg artery imaging was performed first, starting with a 30-s low-dose CT transmission scan (140 kV, 80 mA, 4.25-mm slice thickness) used for localization and attenuation correction. The umbilicus was the upper limit of the scan (approximately coinciding with the aortic bifurcation), which covered 3 bed positions inferiorly. There was a 10-min acquisition in each bed position in 2-dimensional mode. The final 12 patients underwent a modified protocol, which added femoral (down to the knee level) PET/CT to the preexisting carotid and iliac PET/CT. The protocol was achieved by increasing the scan coverage to 4 bed positions (10 min each), with the inferior border of the scan being the patella.

Carotid artery imaging was performed immediately after leg imaging. Patients were placed into a soft head holder, and after another low-dose CT scan, a single–bed-position carotid PET scan was performed in 3-dimensional mode for 15 min. The external auditory meatus was the upper limit of the scan.

Image Reconstruction

The 2-dimensional leg PET data were reconstructed using the ordered-subset expectation maximization algorithm (*10*) with 2 iterations (28 subsets, with corrections applied for normalization, dead time, random events, scatter, attenuation, and sensitivity), yielding a final voxel size of 4.25 mm. The 3-dimensional carotid PET data had the same corrections applied and were reconstructed using a 3-dimensional reprojection algorithm (*11*), giving a voxel size of 4.25 mm.

Image Analysis

Image analysis was performed on a dedicated workstation (Xeleris 2.0; GE Healthcare). We used the CT images, dividing the arteries of the leg anatomically from the aortic bifurcation downward into the iliac and femoral arteries. The common and external iliac arteries were combined and treated together as "iliac artery"; similarly, the common femoral and superficial femoral arteries were amalgamated into the single label of "femoral artery." The transition point between iliac and femoral arteries was the inguinal ligament. Carotid artery PET studies were also quantified by locating the artery using the non–contrast-enhanced CT images.

Arterial ^{18}F-FDG uptake (as a measure of arterial inflammation) in the legs and neck was measured by drawing a region of interest (ROI) around the artery on every slice of the coregistered transaxial PET/CT images (Fig. 1). On each image slice, the mean and maximum standardized uptake values (SUVs) of ^{18}F-FDG in the ROI (containing the arterial wall and the lumen) were

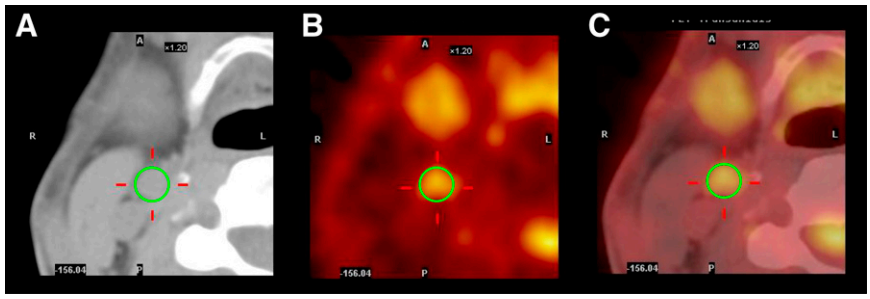

FIGURE 1. Example of image analysis on transaxial CT (A), PET (B), and fused PET/CT (C) images of right carotid artery. Circular ROI is drawn around right carotid artery on CT image. Data from this same ROI on PET image provides mean and maximum SUVs within defined ROI. For each arterial region, this analysis is repeated on all transaxial slices, averaged, and divided by venous SUV to obtain 1 average mean and average maximum TBR, respectively.

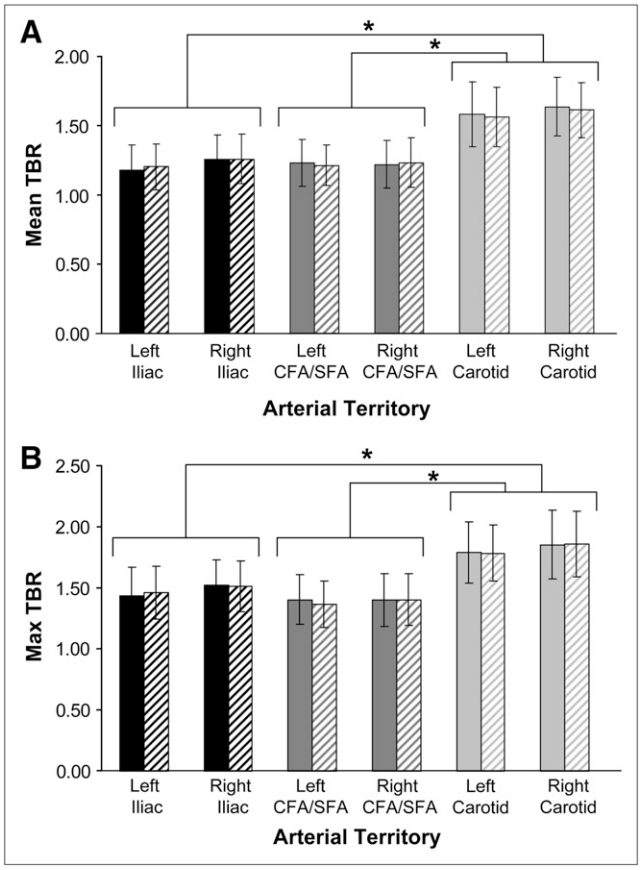

FIGURE 2. Mean (A) and maximum (B) TBR values for each arterial region at day 1 (solid bars) and day 14 (hatched bars). Error bars represent SD values. Within each arterial region, there was no significant difference between TBR values measured at day 1 vs. day 14 for either mean or maximum TBR. At both time points and for both mean and maximum TBR methodologies, TBR in each carotid artery was significantly higher than TBR for iliac and femoral arteries on same side ($P < 0.001$ for all). CFA = common femoral artery; SFA = superficial femoral artery. *$P < 0.001$.

calculated as the mean and maximum pixel activity. The SUV is the decay-corrected tissue concentration of ^{18}F-FDG (in kBq/g), adjusted for injected ^{18}F-FDG dose and body weight (in kBq/g), and is a well-recognized method for quantification of ^{18}F-FDG PET data (*12*).

By averaging SUVs for all artery slices within an arterial territory, we derived mean and maximum SUVs for each region. These SUVs were normalized to blood ^{18}F-FDG activity by division by an average blood ROI (at least 8 venous ROI measurements), estimated from either the inferior vena cava (leg studies) or the jugular vein (carotid studies). This calculation resulted in an arterial TBR measure, which is reported subsequently.

Approximately 240 slices of PET data for each leg study (120 each for left and right) and a total of 36 slices for each carotid study were read.

Assessing Interscan and Intra- and Interobserver Reproducibility

One reader analyzed both studies (scan 1 and scan 2) in every patient. Additionally, intraobserver agreement was assessed. Scan 1 studies of the 19 patients completing the 2 imaging time points were reread by the same reader about 4 wk after the first reading. Interobserver agreement was also assessed by a second experienced reader after the 2 readers had coread several pilot studies (not included in this study) and established a standard protocol for analysis. All image analyses were performed in a masked manner, with studies presented for reading in a random order.

Statistical Methods

Continuous variables are expressed as mean ± SD. Paired, 2-sided Student *t* tests were used to check for differences between mean values of continuous variables. *P* values of less than 0.05 were considered statistically significant. Left and right iliac, femoral, and carotid arteries were treated as individual measurements rather than as one measurement averaged together.

ICCs (*13*) with 95% confidence intervals were calculated to test the interscan variability (1-way random effects model with absolute agreement), and also to assess interobserver (2-way mixed effects model with absolute agreement) and intraobserver agreement (1-way random effects model with absolute agreement), after the methods of McGraw and Wong (*14*). An ICC value of 1 indicates perfect agreement, with random or systematic differences between the 2 measurements decreasing the value of the ICC. Generally, ICC values greater than 0.8 are accepted as a measure of excellent reproducibility (*13*).

Bland–Altman plots (*15,16*), with their corresponding limits of agreement, were drawn to check interobserver, intraobserver, and interscan variability. This visual method allows one to judge

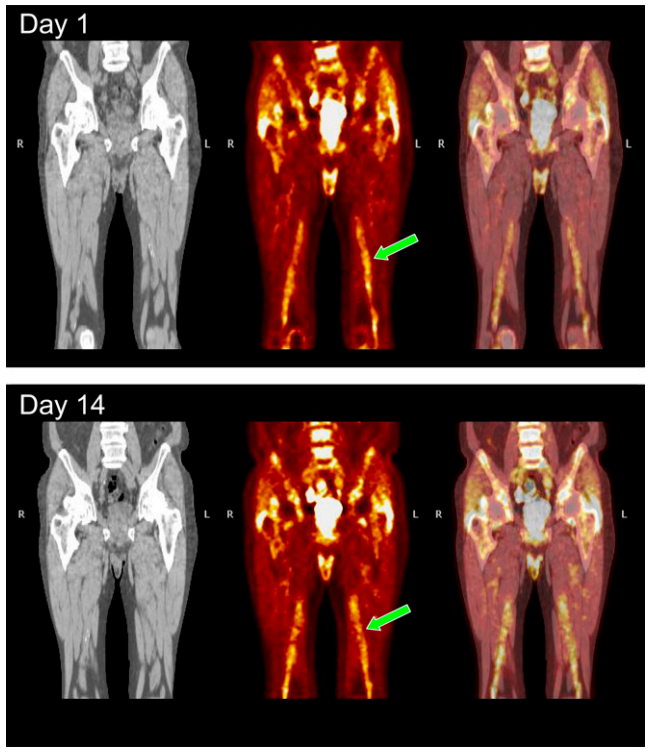

FIGURE 3. Coronal CT (left), ^{18}F-FDG PET (middle), and fused PET/CT (right) images of femoral artery territory at day 1 and day 14. Scans were separated by 2 wk. Note little change in amount of ^{18}F-FDG uptake in femoral artery between 2 scans. Arrows on ^{18}F-FDG PET images highlight femoral artery ^{18}F-FDG accumulation.

TABLE 1
ICC Values Using Mean TBR Measurements

Parameter	Left iliac	Right iliac	Left femoral	Right femoral	Left carotid	Right carotid
Interobserver agreement	0.94 (0.84–0.98)	0.86 (0.68–0.94)	0.88 (0.35–0.97)	0.86 (0.43–0.96)	0.95 (0.88–0.98)	0.96 (0.89–0.98)
Intraobserver agreement	0.96 (0.90–0.98)	0.92 (0.81–0.97)	0.97 (0.89–0.99)	0.95 (0.84–0.99)	0.93 (0.83–0.97)	0.95 (0.90–0.98)
Interscan variability	0.89 (0.74–0.96)	0.85 (0.66–0.94)	0.88 (0.64–0.96)	0.95 (0.85–0.99)	0.89 (0.73–0.95)	0.92 (0.80–0.97)

Data in parentheses are 95% confidence intervals.

agreement across a range of values for continuous variables such as TBR and can highlight systematic measurement bias. The plots consisted of the mean measurement difference plotted against the mean of the 2 measurements. The limit of agreement lines was also calculated and plotted, representing the mean ± 2 SDs of the measurement difference. Statistical analyses were performed using analysis software (SPSS version 14; SPSS Inc.).

RESULTS

Patient Characteristics

The 20 recruited patients had a mean age of 64.9 ± 8.1 y and included 6 women. Patients were clinically stable and asymptomatic when imaged. All had previously documented vascular disease (2 with previous TIAs, 16 with angiographically documented coronary artery disease with prior coronary revascularization, and 2 with prior myocardial infarction) or multiple risk factors for disease (2 patients). Twenty-five percent of the patients had type 2 diabetes.

Imaging Parameters

The mean injected dose of ^{18}F-FDG was not significantly different between scan 1 and scan 2 (mean for scan 1, 567 ± 55 MBq, and mean for scan 2, 596 ± 74 MBq; $P = 0.17$). PET of the legs commenced on average 104 ± 16 min after ^{18}F-FDG injection, and this commencement time was not significantly different between scans (mean for scan 1, 102 ± 14 min, and mean for scan 2, 106 ± 18 min; $P = 0.41$). Similarly, the mean start time for carotid imaging was 148 ± 18 min after injection, with no significant difference between scans (mean for scan 1, 146 ± 18 min, and mean for scan 2, 149 ± 18 min; $P = 0.60$). Prescan glucose levels did not change significantly between scans: 104.2 ± 24.3 mg/dL at scan 1 and 102.4 ± 24.5 mg/dL at scan 2; $P = 0.82$. Although patients' medical records were not obtained, no patient reported any change in symptoms or medications over the 2 wk between imaging sessions.

Mean and maximum TBR uptake values for leg and carotid arteries are shown in Figure 2. The carotid arteries had significantly higher mean and maximum TBR values than did the iliac and femoral arteries at both time points (scan 1 data, mean TBR: $P < 0.001$ for left carotid vs. left iliac artery and $P < 0.001$ for left carotid vs. left femoral artery; scan 1 data, maximum TBR: $P < 0.001$ for left carotid vs. left iliac artery and $P < 0.001$ for left carotid vs. left femoral artery).

Figure 2 also demonstrates no significant change in ^{18}F-FDG signal over the 2-wk period between scans. Figure 3 shows representative images of peripheral artery imaging at day 1 and day 14, with visually little change in ^{18}F-FDG accumulation between the 2 images.

Tables 1 and 2 show the intraclass correlation coefficients, along with their 95% confidence intervals for interobserver, intraobserver, and interscan variability. ICC values calculated for mean TBR are shown in Table 1, and maximum TBR ICC values are shown in Table 2. All mean TBR ICC values are greater than 0.8, with narrow confidence intervals. When maximum TBR is used, the result is an improvement in all measures of reproducibility in the femoral territory, with minor, nonsignificant reductions in the iliac and carotid territories. The carotid territory, as demonstrated by previous studies (*7*), scores high in interobserver agreement, and the TBR level is stable over 2 wk. The femoral artery, which is simple to trace on PET/CT and therefore easy to accurately define for ROI placement, also performs well. For the iliac artery, measures were uniformly good, a surprising result because of its tortuous course within the pelvis.

We constructed Bland–Altman plots to visually examine the reproducibility statistics. Right and left arteries were

TABLE 2
ICC Values Using Maximum TBR Measurements

Parameter	Left iliac	Right iliac	Left femoral	Right femoral	Left carotid	Right carotid
Interobserver agreement	0.90 (0.76–0.96)	0.84 (0.63–0.94)	0.94 (0.80–0.98)	0.94 (0.81–0.98)	0.94 (0.85–0.98)	0.96 (0.90–0.98)
Intraobserver agreement	0.96 (0.91–0.99)	0.92 (0.82–0.97)	0.99 (0.95–1.00)	0.98 (0.92–0.99)	0.88 (0.73–0.95)	0.95 (0.89–0.98)
Interscan variability	0.88 (0.72–0.95)	0.88 (0.72–0.95)	0.95 (0.83–0.98)	0.99 (0.95–1.00)	0.86 (0.69–0.95)	0.91 (0.79–0.96)

Data in parentheses are 95% confidence intervals.

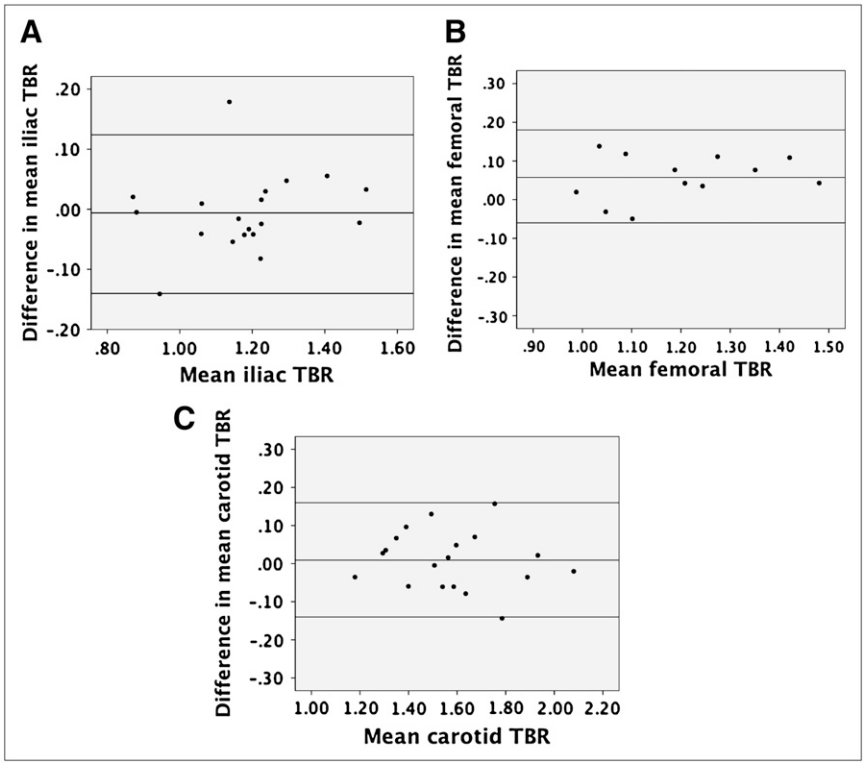

FIGURE 4. Examples of Bland–Altman plots showing interobserver agreement using mean TBR data in left iliac (A), femoral (B), and carotid (C) regions. Difference in TBR measurements between 2 observers does not vary depending on value of TBR, and observers almost always agreed within 2 SDs of measured difference, indicated by horizontal lines on each plot.

considered separately, so plots were constructed for interobserver, intraobserver, and interscan agreement for each right and left arterial territory (a total of 18 plots). Examples for both mean and maximum TBR Bland–Altman plots are shown in Figures 4 and 5. All plots displayed narrow scatter (defined by most data points lying within 2 SDs of the mean difference in TBR) and confirmed the absence of systematic measurement bias. The range of the mean and maximum differences is plotted in the figures (between 0.12 and 0.17 for mean TBR measurements and between 0.16 and 0.20 for maximum TBR measures).

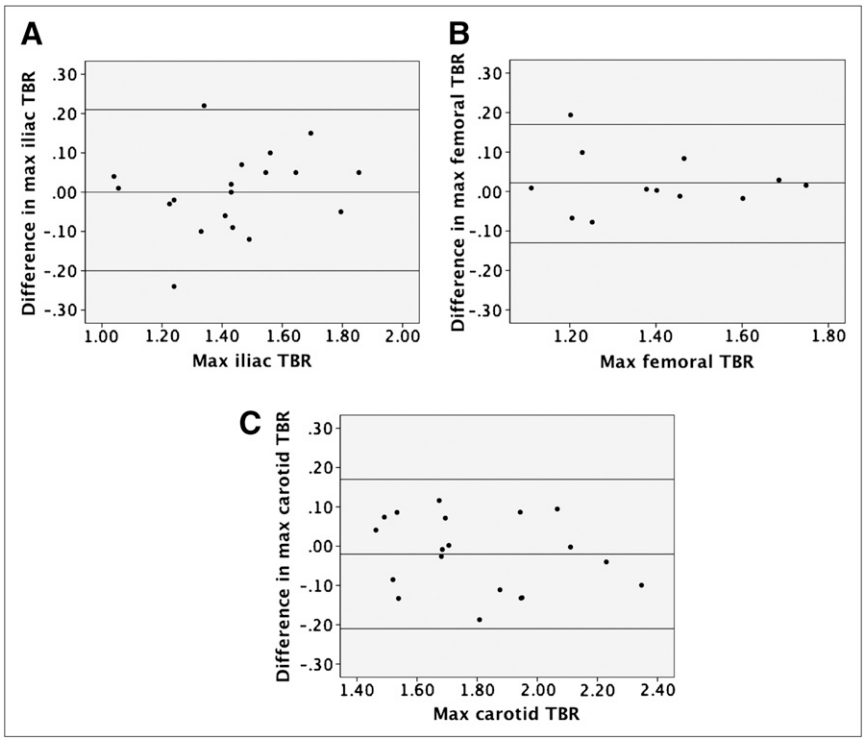

FIGURE 5. Examples of Bland–Altman plots showing interobserver agreement using maximum TBR data in left iliac (A), femoral (B), and carotid (C) regions. Difference in TBR measurements between 2 observers does not vary depending on value of TBR, and observers almost always agreed within 2 SDs of measured difference, indicated by horizontal lines on each plot. Max = maximum.

TABLE 3
Published Studies of ^{18}F-FDG PET Atherosclerosis Imaging

References	Imaging	Population studied	Circulation time and mode of imaging	^{18}F-FDG uptake measure	Vessel activity normalization	Significance
17	PET + CCT	Symptomatic carotid disease	Late imaging (190 min)	^{18}F-FDG accumulation rate	Blood	Symptomatic plaques more metabolically active than asymptomatic lesions
20	PET + MRI	Symptomatic carotid disease	Dynamic (120 min) (last 30 min used for quantification)	Plaque-to-normal vessel uptake ratio	Muscle	Vertebral arteries imaged
21	PET + CCT or MRI	Symptomatic carotid disease	90 min	Vessel mean and maximum SUV	Blood	Subclavian and brachiocephic arteries imaged
6	PET + CCT or MRI	Carotid disease	Late imaging (180 min)	Vessel and plaque maximum SUV	Blood	Correlation ^{18}F-FDG with macrophage content of plaque
25	PET + CCT	Cancer screening	Late imaging (60 min)	Vessel maximum SUV	Not performed	Statin intervention study
24	PET + CCT	Cancer screening	Late imaging (60 min)	Vessel maximum SUV	Not performed	100 patients imaged
19	Combined PET/CT	Carotid disease	Early (45 min) and late (150 min)	Plaque maximum SUV	Not performed	MMP-1 correlation with ^{18}F-FDG uptake
18	PET + x-ray angiography	Symptomatic carotid disease	Dynamic (90 min) (last 30 min used for quantification)	Plaque SUV (maximum/mean not stated)	Not performed	^{18}F-FDG uptake proportional to stenosis severity
7	Combined PET/CT	Spectrum of patients with coronary and carotid disease	Late (90 min)	Vessel mean SUV	Blood	High reproducibility in carotid artery and aorta

CCT = contrast-enhanced CT.

DISCUSSION

We have shown for, what is to our knowledge, the first time reproducible uptake of ^{18}F-FDG within the arteries of the pelvis and legs and confirmed reproducible uptake in the carotid arteries, in a relatively large cohort of patients. Additionally, we have compared 2 methods of ^{18}F-FDG uptake in this study, mean and maximum TBR, and have found that the 2 methods are approximately equally effective in terms of reproducibility.

Previously Published ^{18}F-FDG PET Studies

Table 3 provides information on significant published studies of ^{18}F-FDG PET for vascular imaging. The table highlights the wide range of choices that have been made by investigators on PET scan acquisition mode, ^{18}F-FDG circulation time, and the decision to normalize the artery/plaque ^{18}F-FDG signal to background structures.

The first attempt at atherosclerosis imaging with ^{18}F-FDG PET used a stand-alone PET scanner along with contrast-enhanced CT for anatomic coregistration (*17*). Eight patients with TIA were imaged shortly after their index events. Significantly more ^{18}F-FDG accumulated within symptomatic plaques than in the contralateral asymptomatic arteries. The cellular fate of ^{18}F-FDG taken up by cells in the plaques was not clear, and so autoradiography using tritiated deoxyglucose was performed on excised plaques from the same group of symptomatic patients. This revealed that the majority of deoxyglucose was within plaque macrophages. The relationship between the degree of ^{18}F-FDG uptake into plaque, clinical symptoms, macrophage burden, and level of serum inflammatory markers has recently been confirmed in much larger patient groups (*6,18,19*).

Animal studies also show strong positive correlations between ^{18}F-FDG uptake and plaque macrophage burden. Several arterial beds have now been successfully imaged with ^{18}F-FDG PET. These include the vertebral arteries (*20*), brachial and subclavian arteries (*21*), and all regions of the aorta (*22,23*) of patients with either established vascular disease or risk factors for it (*24*). One recent publication has even been able to localize ^{18}F-FDG uptake to regions of the coronary arteries, suggesting possible uptake within coronary atherosclerosis (*22*), although this remains to be confirmed. Finally, 1 group has been able to track regression of atherosclerotic inflammation during statin therapy (*25*).

Recommendations for Future Studies

More uniform methodology is needed if atherosclerosis imaging with ^{18}F-FDG PET is to be widely adopted. Because excellent reproducibility has been shown in the carotid arteries, the ascending aorta (*7*), and now the peripheral arteries, we suggest that an acquisition protocol similar to that published here and in previous papers (*6,7*) should be adopted. It appears from dynamic studies (*20*) that uptake of ^{18}F-FDG occurs over a longer time course in

arteries than in tumors, so a longer ^{18}F-FDG circulation time is recommended, preferably at least 90 min. The use of combined PET/CT scanners is also desirable for several reasons, including ease of coregistration of the PET and CT images, faster scan times (a separate transmission scan is not required), and the wide availability of combined scanners as part of cancer-imaging programs (*26*).

We suggest that for trials of systemic therapies aimed at arterial inflammation (e.g., statin drugs), the mean TBR measurement across a substantial portion of the artery be used, as the drug effect is likely to be spread across the arterial bed. However, for testing therapies that act locally on the plaque, such as vulnerable plaque stent implantation or gene therapy, a more appropriate method might be to track the maximum TBR measurement within the localized disease segment over time. This recommendation is in line with a recent publication examining this issue in oncology (*27*).

Advancements in scanner hardware, such as time-of-flight imaging and high-definition PET, as well as the likely appearance in the marketplace of combined PET and MRI machines should improve quantification by straightforward partial-volume correction and lower both scan time and radiation dose. Further improvements in isolating the SUV measurement from the arterial wall, such that the ROI does not include the arterial lumen, might also improve accuracy.

Other Novel Imaging Approaches

Finally, 2 other noninvasive imaging techniques aimed at quantifying macrophage activity have also emerged over the last few years and deserve mention. Preclinical work suggests that macrophage-targeted CT contrast agents (*28*) may have a role in detecting and assessing novel drug treatments against the vulnerable plaque. This platform may allow coronary artery inflammation imaging, a goal that is currently out of reach of ^{18}F-FDG PET. Human studies using high-resolution MRI with ultrasmall superparamagnetic iron oxide contrast have been shown to detect symptomatic plaque in the carotid territories of patients with recent TIA (*29–31*).

Both of these methods have advantages and disadvantages when compared with ^{18}F-FDG PET of atherosclerosis, and a combination of different techniques for coronary, carotid, and aortic vascular beds is likely to be required.

CONCLUSION

^{18}F-FDG PET of carotid and peripheral artery atherosclerosis is highly reproducible over 2 wk and between readers. We suggest the adoption of standardized imaging and analysis protocols to allow further testing of this novel technique in the assessment of drugs and devices aimed at the high-risk atherosclerotic plaque.

ACKNOWLEDGMENTS

This work was funded by grants from the National Institutes of Health/National Heart, Lung and Blood (R01 HL71021, R01 HL78667) and by an unrestricted research grant from Merck Research Laboratories. One of the authors (KM) was supported by the Doris Duke Charitable Foundation, and another (JR) is supported by an International Fellowship from the British Heart Foundation.

REFERENCES

1. Pasternak RC, Criqui MH, Benjamin EJ, et al. Atherosclerotic Vascular Disease Conference: writing group I: epidemiology. *Circulation.* 2004;109:2605–2612.
2. Grundy SM, Cleeman JI, Merz CN, et al. Implications of recent clinical trials for the National Cholesterol Education Program Adult Treatment Panel III guidelines. *Circulation.* 2004;110:227–239.
3. Naghavi M, Libby P, Falk E, et al. From vulnerable plaque to vulnerable patient: a call for new definitions and risk assessment strategies: Part II. *Circulation.* 2003;108:1772–1778.
4. Greenland P, LaBree L, Azen SP, Doherty TM, Detrano RC. Coronary artery calcium score combined with Framingham score for risk prediction in asymptomatic individuals. *JAMA.* 2004;291:210–215.
5. Davies MJ. Acute coronary thrombosis—the role of plaque disruption and its initiation and prevention. *Eur Heart J.* 1995;16(suppl L):3–7.
6. Tawakol A, Migrino RQ, Bashian GG, et al. In vivo ^{18}F-fluorodeoxyglucose positron emission tomography imaging provides a noninvasive measure of carotid plaque inflammation in patients. *J Am Coll Cardiol.* 2006;48:1818–1824.
7. Rudd JH, Myers KS, Bansilal S, et al. ^{18}Fluorodeoxyglucose positron emission tomography imaging of atherosclerotic plaque inflammation is highly reproducible: implications for atherosclerosis therapy trials. *J Am Coll Cardiol.* 2007;50:892–896.
8. Mahmud E, Cavendish JJ, Salami A. Current treatment of peripheral arterial disease: role of percutaneous interventional therapies. *J Am Coll Cardiol.* 2007;50:473–490.
9. Ramaiah V, Gammon R, Kiesz S, et al. Midterm outcomes from the TALON registry: treating peripherals with SilverHawk: outcomes collection. *J Endovasc Ther.* 2006;13:592–602.
10. Gundlich B, Musmann P, Weber S, Nix O, Semmler W. From 2D PET to 3D PET: issues of data representation and image reconstruction. *Z Med Phys.* 2006;16:31–46.
11. Kinahan PE, Rogers JG. Analytic 3D image reconstruction using all detected events. *IEEE Trans Nucl Sci.* 1989;36:964–968.
12. Shankar LK, Hoffman JM, Bacharach S, et al. Consensus recommendations for the use of ^{18}F-FDG PET as an indicator of therapeutic response in patients in National Cancer Institute trials. *J Nucl Med.* 2006;47:1059–1066.
13. Eliasziw M, Young SL, Woodbury MG, Fryday-Field K. Statistical methodology for the concurrent assessment of interrater and intrarater reliability: using goniometric measurements as an example. *Phys Ther.* 1994;74:777–788.
14. McGraw KO, Wong SP. Forming inferences about some intraclass correlation coefficients. *Psychol Methods.* 1996;1:30–46.
15. Bland JM, Altman DG. Statistical methods for assessing agreement between two methods of clinical measurement. *Lancet.* 1986;1:307–310.
16. Bland JM, Altman DG. Applying the right statistics: analyses of measurement studies. *Ultrasound Obstet Gynecol.* 2003;22:85–93.
17. Rudd JHF, Warburton EA, Fryer TD, et al. Imaging atherosclerotic plaque inflammation with [^{18}F]-fluorodeoxyglucose positron emission tomography. *Circulation.* 2002;105:2708–2711.
18. Arauz A, Hoyos L, Zenteno M, Mendoza R, Alexanderson E. Carotid plaque inflammation detected by ^{18}F-fluorodeoxyglucose-positron emission tomography pilot study. *Clin Neurol Neurosurg.* 2007;109:409–412.
19. Wu YW, Kao HL, Chen MF, et al. Characterization of plaques using ^{18}F-FDG PET/CT in patients with carotid atherosclerosis and correlation with matrix metalloproteinase-1. *J Nucl Med.* 2007;48:227–233.
20. Davies JR, Rudd JH, Fryer TD, et al. Identification of culprit lesions after transient ischemic attack by combined ^{18}F fluorodeoxyglucose positron-emission tomography and high-resolution magnetic resonance imaging. *Stroke.* 2005;36:2642–2647.
21. Okane K, Ibaraki M, Toyoshima H, et al. ^{18}F-FDG accumulation in atherosclerosis: use of CT and MR co-registration of thoracic and carotid arteries. *Eur J Nucl Med Mol Imaging.* 2006;33:589–594.
22. Dunphy MP, Freiman A, Larson SM, Strauss HW. Association of vascular ^{18}F-FDG uptake with vascular calcification. *J Nucl Med.* 2005;46:1278–1284.

23. Tatsumi M, Cohade C, Nakamoto Y, Wahl RL. Fluorodeoxyglucose uptake in the aortic wall at PET/CT: possible finding for active atherosclerosis. *Radiology.* 2003;229:831–837.
24. Tahara N, Kai H, Yamagishi S, et al. Vascular inflammation evaluated by [^{18}F]-fluorodeoxyglucose positron emission tomography is associated with the metabolic syndrome. *J Am Coll Cardiol.* 2007;49:1533–1539.
25. Tahara N, Kai H, Ishibashi M, et al. Simvastatin attenuates plaque inflammation: evaluation by fluorodeoxyglucose positron emission tomography. *J Am Coll Cardiol.* 2006;48:1825–1831.
26. Weber WA, Figlin R. Monitoring cancer treatment with PET/CT: does it make a difference? *J Nucl Med.* 2007;48(suppl):36S–44S.
27. Teo BK, Seo Y, Bacharach SL, et al. Partial-volume correction in PET: validation of an iterative postreconstruction method with phantom and patient data. *J Nucl Med.* 2007;48:802–810.
28. Hyafil F, Cornily JC, Feig JE, et al. Noninvasive detection of macrophages using a nanoparticulate contrast agent for computed tomography. *Nat Med.* 2007;13:636–641.
29. Kooi ME, Cappendijk VC, Cleutjens KB, et al. Accumulation of ultrasmall superparamagnetic particles of iron oxide in human atherosclerotic plaques can be detected by in vivo magnetic resonance imaging. *Circulation.* 2003;107:2453–2458.
30. Trivedi R, King-Im J, Gillard J. Accumulation of ultrasmall superparamagnetic particles of iron oxide in human atherosclerotic plaque [letter]. *Circulation.* 2003;108:e140.
31. Tang TY, Howarth SP, Miller SR, et al. Comparison of the inflammatory burden of truly asymptomatic carotid atheroma with atherosclerotic plaques contralateral to symptomatic carotid stenosis: an ultra small superparamagnetic iron oxide enhanced magnetic resonance study. *J Neurol Neurosurg Psychiatry.* 2007;78:1337–1343.